

Hexagonal Meshes with Planar Faces

Wenping Wang, Yang Liu, Dongming Yan, Bin Chan, Ruotian Ling, Feng Sun
Department of Computer Science, The University of Hong Kong

(HKU CS Technical Report, *TR-2008-13*)

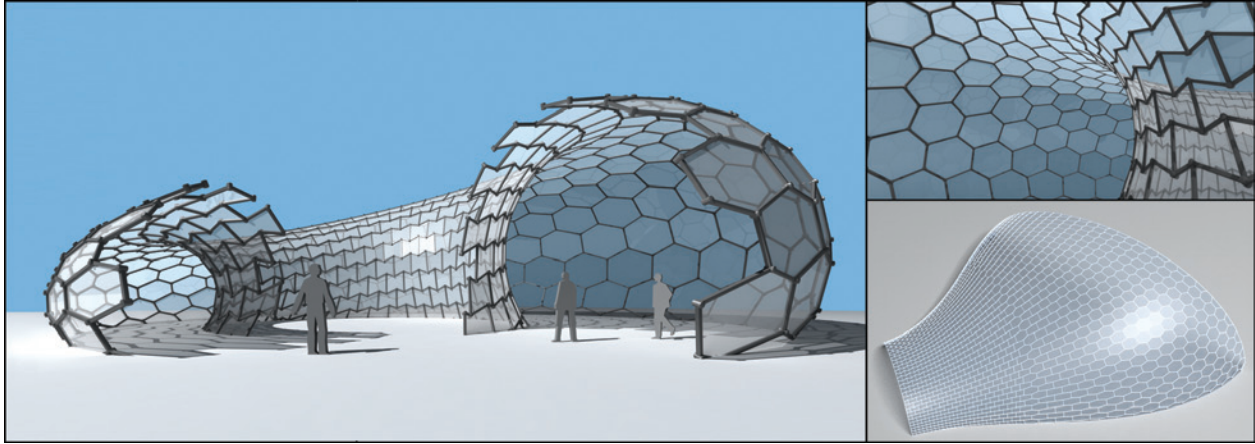


Figure 1: (Left): A conceptual architectural structure as a *P-Hex* mesh, computed using the progressive conjugation method. The interior view (top right) shows that the shapes of the *P-Hex* faces transit smoothly across the parabolic curve. (Bottom right): another *P-Hex* mesh of free form shape.

Abstract

Free-form meshes with planar hexagonal faces, to be called *P-Hex meshes*, provide a useful surface representation in discrete differential geometry and are demanded in architectural design for representing surfaces built with planar glass/metal panels. We study the geometry of *P-Hex* meshes and present an algorithm for computing a free-form *P-Hex* mesh of a specified shape. Our algorithm first computes a regular triangulation of a given surface and then turns it into a *P-Hex* mesh approximating the surface. A novel local duality transformation, called *Dupin duality*, is introduced for studying relationship between triangular meshes and for controlling the face shapes of *P-Hex* meshes.

This report is based on the results presented at Workshop "Polyhedral Surfaces and Industrial Applications" held on September 15-18, 2007 in Strobl, Austria.

CR Categories: I.3.5 [Computer Graphics]: Computational Geometry and Object Modeling—Geometric algorithms, languages, and systems; I.3.5 [Computer Graphics]: Computational Geometry and Object Modeling—Curve, surface, solid, and object representations

Keywords: planar hexagonal mesh, Dupin duality, surfaces in architecture, discrete differential geometry

1 Introduction

The increasing demand in architecture for modeling freeform surfaces built with planar glass/metal panels provides motivations and challenges for studies on mesh surfaces with planar faces, also called *polyhedral surfaces* [Pottmann et al. 2007a]. In this paper we focus on the geometry and computation of *mesh surfaces with planar hexagonal faces*. Such meshes will be called *P-Hex meshes* for short.

Computing a *P-Hex* mesh is equivalent to tiling a surface with planar hexagons, which is an extension to the classical plane tiling problem. Tiling the plane with regular patterns has been well studied in 2D crystallography [Coxeter 1989] and a comprehensive exposition on general plane tiling can be found in [Grunbaum and Shephard 1986]. If only the congruent copies of a regular polygon are to be used then the plane can only be tiled with equilateral triangles, squares, or regular hexagons. With an affine transformation, the plane can also be tiled with congruent affine copies of these three regular polygons. There are also other types of plane tiling that use non-regular polygons or more than one type of tiles.

The problem of tiling a surface with the same type of polygons is more challenging than its counterpart in the plane. In general, one can no longer require the tiles to be identical – the variation of face shapes is inevitable since they are constrained by surface curvature. Such constraints by surface curvature can be quite significant. For

example, as we shall, a negatively curved surface cannot be tiled by a mesh of planar convex polygons with valence-3 vertices.

In architectural construction, glass panels represented by planar faces of a mesh surface are framed by beams joined at nodes (also known as *junctions*) where all adjacent faces meet each other. A major consideration of manufacturing cost is to reduce the node complexity, i.e., the number of beams joined at a node. Although a triangle mesh with vertices of valence 6 meets the face planarity requirement naturally, it has the most complex nodes, so is often not preferred in practice. Another disadvantage of the triangle mesh is that it does not have a proper definition of offset meshes [Pottmann et al. 2007b].

This leads to demands for free-form meshes with planar quadrilateral faces (or *P-Quad meshes*) and mesh surfaces with planar hexagonal faces (or *P-Hex meshes*), as extensions to plane tiling with squares and regular hexagons. The geometry and effective computation of P-Quad meshes are well known [Sauer 1970; Liu et al. 2006]: the edges of a P-Quad mesh are discretization of conjugate curve networks of the underlying smooth surface. Various special P-Quad meshes have also been identified. For example, if a P-Quad mesh is required to possess a constant face-distance offset, then it belongs to the special class of *conical P-Quad meshes* which discretize curvature lines of the underlying smooth surface [Liu et al. 2006].



Figure 2: Left: A buckyball – the molecule Carbon 540; right: the hexagonal roof in Eden project.

P-Hex meshes are an attractive shape representation for several reasons. The hexagonal tiling or hexagonal symmetry arises naturally in organic structures, such as honeycomb, the epidermal layer of cells and the beautiful skeleton of radiolaria revealed by Ernst Haeckel [Thompson 1992], appears as the predominant structure in fullerene-like graphite structure (e.g., buckyballs and nanotubes – see Figure 2) [Harris 1999], and is the optimal layout for tightest circle packing in the plane [Coxeter 1989]. Therefore it is regarded as a highly harmonious and symmetric shape with natural visual appeal [Weyl 1983]. For surface modeling in architecture, P-Hex meshes have the simplest node, since there are only three beams joining at each node; furthermore, any P-Hex mesh is a *conical mesh*, thus possessing constant face-distance offset meshes to facilitate the modeling of multilayered surface structure [Liu et al. 2006]. Finally, P-Hex meshes provide a useful shape representation in discrete differential geometry [Bobenko and Suris 2005] – their offset property allows simple and elegant definition and computation of surface curvature for the purpose of modeling various special surface (e.g., minimal surfaces and constant mean curvature surfaces) [Bobenko et al. 2006; Pottmann et al. 2007b; Mueller 2007].

However, there has been little research in the literature about the geometry or computation of free-form P-Hex meshes. Almost all building surfaces modeled with P-Hex meshes seen in real life, known as *geodesic domes* [Tarnai 1993], are spherical, such as the *Eden Project* in UK (see Figure 2). We fill this gap by studying the geometry of P-Hex meshes and giving the first method for computing free-form P-Hex meshes.

Contribution Our contributions are the following.

1. We reveal a natural correspondence between regular triangle meshes and P-Hex meshes, and develop a novel analytical tool, called *Dupin duality*, to study this correspondence for controlling the shape of the hexagonal faces in the computation of P-Hex meshes. We emphasize on the shape, size and pattern of the mesh faces and study how these criterions are affected by surface curvatures and various conjugate curve networks.
2. We present a complete and robust method that computes a valid triangle meshes approximating a given free-form surface and uses Dupin duality and nonlinear optimization to turn it into a P-Hex mesh with desired face shape and pattern.

2 Related work

Much work has been done in surface remeshing using quad meshes (e.g., [Alliez et al. 2003; Marinov and Kobbelt 2004; Kälberer et al. 2007]) and subdivision for generating hexagonal meshes [Oswald and Schröder 2003], without seeking the planarity of the faces. Planar quad meshes are the topic of [Glymph et al. 2004; Liu et al. 2006] from the viewpoint of building construction. General meshes with planar faces are computed in [Cohen-Steiner et al. 2004; Cutler and Whiting 2006] without control over the number of sides or the shape of the faces. The offset properties of P-Hex meshes are investigated in [Pottmann et al. 2007b]. Muller [Mueller 2007] considers using hexagons for constructing minimal surfaces via the technique of parallel meshes. In chemistry, tiling free form surfaces with polygons, which are in general non-planar, is of great importance to finding fullerenes beyond buckyballs and nano-tubes [Terrones and Mackay 1992; Tarnai 1993].

Projective duality establishes a correspondence between P-Hex meshes in prime space and triangle meshes in dual space. This relationship has been explored by Kawaharada and Sugihara [Kawaharada and Sugihara 2006] to derive subdivision rules for P-Hex meshes from subdivision rules for triangle meshes. However, when applied to computing a P-Hex mesh of a given shape S from a triangle mesh of the dual of S , the projective duality suffers from high metric distortion and not being a one-to-one correspondence for a free-form shape, since surface points with the same tangent planes are mapped to the same point. All these cause unstable computation, as well as self-intersection and shape distortion of the faces of the resulting P-hex mesh.

For a given surface S , Almegaard et al. [Almegaard et al. 2007] use a piecewise linear supporting function of S over the Gauss sphere S^2 to compute a P-Hex mesh. Since the supporting function is the composition of a projective duality and the inversion with respect to a sphere, this method basically suffers from the same problems of the approach above based on projective duality, especially the issues of self-intersecting faces of P-Hex meshes. In particular, it is unclear with this method what triangulation of S^2 will lead to a P-Hex whose faces are free of self-intersection. Pottmann et al. [Pottmann et al. 2007b] compute a P-Hex mesh of a surface as a parallel mesh of another given P-hex mesh approximating a sphere S^2 . This method does not work for free-form surfaces and often produces self-intersecting P-Hex faces even for simple convex shapes.

Diáz et al. [Severiano et al. 2005] use stereographic projection of power diagrams in 2D to generate polyhedral surfaces, including P-Hex meshes, approximating spheres and their projective equivalents. This method, however, cannot be extended to shapes other than elliptic quadrics or more general surfaces.

To summarize, the major issues with the existing methods that we

need to address are *generality* and *face shape control*, which mean the ability of representing a general free-form shape with P-Hex meshes and the need to ensure that the resulting P-Hex faces are free of self-intersection.

3 Preliminaries

Although it is tempting to tile a free-form surface using planar convex polygons only, a negatively curved surface, such as a hyperboloid of one sheet, cannot be tiled properly by convex planar polygons, supposing that all the interior vertices have valence 3. For example, regular (hence convex) pentagons and heptagons, in addition to regular hexagons, are used to design graphite structure of freeform shapes with valence-3 vertices [Terrones and Mackay 1992; Tarnai 1993]. However, these seemingly convex polygons cannot all be planar in a negatively curved region; in fact, their sides are curves that are realized by bent C-C bonds [Tarnai 1993]. This can be seen as follows.

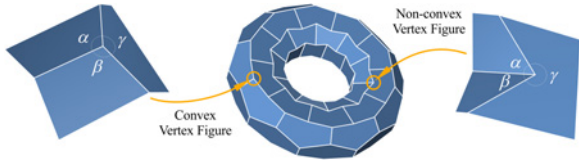


Figure 3: A convex vertex and non-convex vertex on a torus-shaped P-Hex mesh.

Suppose that a negatively curved surface S is approximated by a polyhedral mesh \mathcal{M} with convex faces and valence-3 interior vertices only. For any interior vertex p of \mathcal{M} , three planar faces of \mathcal{M} meet at p . Suppose that the three faces have strictly convex corners at p , i.e., $\alpha, \beta, \gamma < \pi$ (see Figure 3, left). Clearly, $\alpha + \beta + \gamma \leq 2\pi$. We assume that $\alpha + \beta + \gamma \neq 2\pi$, since otherwise the three faces would be coplanar, which would then force the entire mesh \mathcal{M} to be on a plane. Therefore the three faces form a *convex vertex figure* at p , which is characterized by the convex spherical triangle cut out by the three faces on a sphere centered at p . Since the convex figures at all the vertices of \mathcal{M} are consistently oriented, \mathcal{M} is then necessarily a convex surface, contradicting that \mathcal{M} approximates the negatively curved surface S . Hence, at least one concave angle (e.g., $\gamma > \pi$) has to be involved to form a non-convex vertex figure for tiling a negatively curved surface (Figure 3, right). In the following we shall show more specifically how a face of P-Hex mesh is constrained by surface curvature.

Dupin indicatrix An important concept to be used in our investigation is the Dupin indicatrix [Carmo 1976]. Given a surface S and a point $p \in S$, let $T_p(S)$ denote the tangent plane of S at p . Consider a 2D local coordinate system on $T_p(S)$ with the x and y axes aligned with the principal curvature directions of S at p . Then the Dupin indicatrix is the collection of conics defined by $\kappa_1 x^2 + \kappa_2 y^2 = \pm 1$, where κ_1, κ_2 are the principal curvatures of S at p (Figure 4, left). Intuitively, a plane that is near and parallel to $T_p(S)$ cuts S in a shape which in a first approximation similar to the Dupin indicatrix [Struik 1988] (Figure 4, right). When p is an elliptic point, the Dupin indicatrix is the ellipse $\kappa_1 x^2 + \kappa_2 y^2 = 1$, assuming $\kappa_1 > 0$ and $\kappa_2 > 0$ by changing the normal orientation of S if necessary. When p is a hyperbolic point, the Dupin indicatrix consists of two hyperbolas having the same pair of asymptotic lines. When p is a parabolic point, assuming that $\kappa_1 \neq 0$ and $\kappa_2 = 0$, the Dupin indicatrix is a pair of lines $\kappa_1 x^2 = \pm 1$. The Dupin indicatrix is not defined at a planar point, i.e., if $\kappa_1 = \kappa_2 = 0$.

Recall that a *homothetic transformation* in 2D is $x' = ax + c_1$ and

$y' = ay + c_2$, i.e., the composition of a uniform scaling and translation [Coxeter 1989]. Throughout the paper we shall frequently refer to a conic *homothetic* to the Dupin indicatrix. For brevity, we shall call it a *Dupin conic*, or *Dupin ellipse* or *Dupin hyperbola* if we need to be specific. Thus, by a Dupin conic of S at p we will mean a homothetic copy of the Dupin indicatrix of S at p .

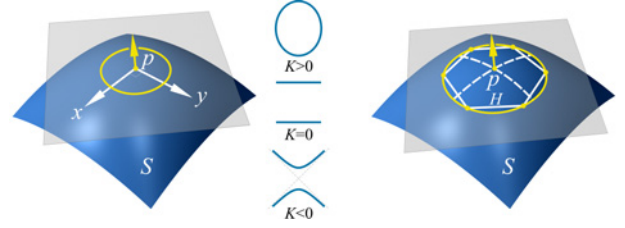


Figure 4: Dupin indicatrix.

To show the constraint of surface curvatures on the shape of a P-Hex face, we first consider the special case where a face f of a P-Hex mesh H , called a *P-Hex face*, has all its vertices on a locally convex surface S . Let P be the plane containing f . (See Figure 4, right.) Since f is inscribed in the curve C on S cut out by P , its vertices are nearly on a Dupin conic. This observation holds in general, that is, for any P-Hex mesh H approximating a free-form S , whose vertices are not necessarily on S , the P-Hex faces of H are approximately inscribed in a Dupin conic. To exclude pathological cases, we suppose that S is approximated by H smoothly in the sense that the approximation error is $O(h^2)$ when the size of P-Hex faces of H is $O(h)$. The exact statement in terms of the order of approximation error is given in the next proposition. Its proof is omitted due to the limitation of space.

Proposition 1 Let H be a P-Hex mesh approximating a surface S . Suppose that f is a face of H and f approximates S at a point $p \in S$, where the principal curvatures of S are not both zero. Let the size of f be $O(h)$. Then the vertices of f have the distances of order $O(h^2)$ to a Dupin conic C of S at p .

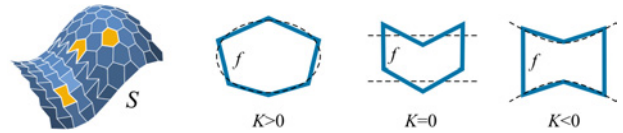


Figure 5: A P-Hex face approximating S is in a approximation inscribed in a Dupin conic.

As a consequence of Proposition 1, if we suppose that the P-Hex face f is a simple polygon, then f is a convex hexagon at an elliptic point of S , since it is approximately inscribed in an ellipse, and a non-convex hexagon at a hyperbolic point of S , since it is approximately inscribed in a hyperbola (Figure 5). The case of $K = 0$ (i.e., parabolic points) deserves special attention. When the parabolic points are isolated or form a parabolic curve, then the P-Hex face at the point or the curve can assume various shapes, as influenced by the neighboring P-Hex faces where $K \neq 0$ (Figure 5).

If $K = 0$ everywhere on the surface S , then S is either a plane or a developable surface, which is necessarily singly curved [Carmo 1976]. When S is a plane, Proposition 1 does not apply, since the Dupin indicatrix is not defined, and in this case any hexagonal mesh of S is a P-Hex mesh. When S is a developable, a P-Hex mesh of S must be very special – all its faces have the shape of a quadrilateral and they are tiled along the rulings of S , as constrained by the degenerate Dupin conics, which are pairs of lines. (The figure on the right shows a P-Hex tiling of a cylinder.)



4 Dupin duality

4.1 Triangle meshes and Dupin dual

In this section we shall first discuss a correspondence, called *tangent duality*, between a *regular triangulation* of a surface S and a P-Hex mesh of S , and then introduce *the Dupin duality* to study the local property of tangent duality. A *regular triangulation* of S , also called a *regular triangle mesh*, refers to a triangle mesh whose vertices are of valence 6. We make the smoothness assumption throughout that the edges of a regular triangulation of S are discretizations of three families of smooth curves on S . In this section we assume that the Gaussian curvature $K \neq 0$. The handling of degenerate cases with $K = 0$ will be discussed in detail in Section 5.3.

Tangent duality Consider a sufficiently dense regular triangle mesh T whose vertices are on a smooth surface S (Figure 6, left). Let t be a triangle of T with vertices v_a, v_b and v_c . Then, in general, the three tangent planes of S at v_a, v_b and v_c intersect at a point. Let us denote this intersection point as u_t and associate it with the triangle t . If we do this for every triangle t of T and connect the points u_t of adjacent triangles of T , then we obtain a hexagonal mesh H combinatorially dual to T (Figure 6, right). Clearly, each face of H is a planar hexagon tangent to S at a vertex of T . Hence, H is a P-Hex mesh approximating S . Conversely, a P-Hex H with its faces tangent to the surface S corresponds to a regular triangle mesh whose vertices are at the tangency points of the faces H with S . This correspondence between T and H will be referred to as the *tangent duality*.

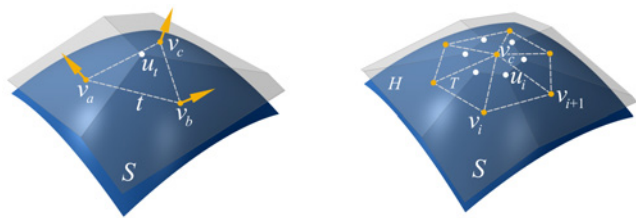


Figure 6: (Left) *Tangent duality*: a vertex u_t of a P-Hex face is at the intersection of three tangent planes of S ; (right) a P-Hex face is obtained from a triangle mesh of S .

Although the tangent duality involves only a straightforward geometric construction, its behavior can be rather complex. There are several questions that must be answered before it can be put in practical use for computing a P-Hex mesh from a triangle mesh. First, under the tangent duality a triangle mesh of a surface S may correspond to a P-hex mesh whose faces have self-intersection. For example, Figure 11(top) shows a triangle mesh of a one-sheet hyperboloid and its corresponding P-Hex mesh with face self-intersection. Hence, the question is how to identify and design those ‘good’ triangle meshes that produce valid P-Hex meshes free

of face self-intersection. Furthermore, we need to know how to find a triangle mesh that, under the tangent duality, corresponds to a P-Hex mesh whose faces have desired shapes. Finally, there is a robustness issue. The tangent duality construction breaks down when the three tangent planes are nearly parallel to each other, either because the three vertices of the triangle t are too close to each other or because the curvature of S is too small. This is a critical problem when we deal with freeform shapes containing parabolic points or nearly planar regions. We will address these issues in the framework of Dupin duality, a new concept to be introduced below.

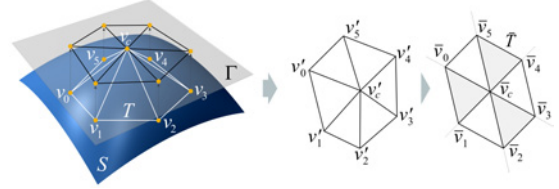


Figure 7: *Dupin duality*: projections of triangle mesh vertices on the tangent plane Γ of S .

Dupin duality Dupin duality is a simple transformation that locally characterizes the behavior of the tangent duality construction. Suppose that T is a regular triangle mesh whose vertices are on a surface S . Let Γ be the tangent plane of S at a vertex $v_c \in S$ of T . Let $v'_i, i = 0, 1, \dots, 5$, be the vertical projections on the plane Γ of the six vertices v_i of T that are connected to v_c (Figure 7, left and middle). Since $v_c \in \Gamma$, its projection on Γ is $v'_c = v_c$. Let t'_i denote the triangles $\Delta v_c v'_i v'_{i+1}, i = 0, 1, \dots, 5, \text{ mod } 6$. Let the size of the triangle t'_i be $O(h)$. By the smoothness assumption on the edges of T , with a perturbation of order $O(h^2)$ the points v'_i can be perturbed into new points \bar{v}_i such that the $\bar{v}_i, i = 0, 1, \dots, 5$, form a centrally symmetric hexagon centered at $\bar{v}_c \equiv v_c$ with all the triangles $\bar{t}_i : v_c \bar{v}_i \bar{v}_{i+1}$ being congruent to each other (Figure 7, right). We call such a group of six triangles \bar{t}_i with the above properties a *triangle star*, and denote it as \bar{T} . Since the six triangles of \bar{T} are congruent, we may pick any one of them and call it the *fundamental triangle*, denote it as \bar{t} .

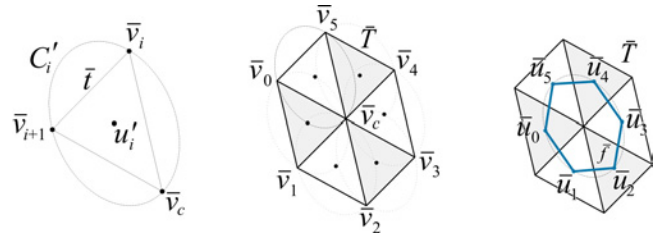


Figure 8: *Dupin duality*. (Left) the Dupin center of the fundamental triangle \bar{t} ; (middle) the Dupin conics of the six triangles in \bar{T} ; (right) the dual hexagon, inscribed in a Dupin conic.

Let C denote the Dupin indicatrix of S at v_c . Since a homothetic transformation in the plane has three free parameters (one for similitude and two for translation), there is a unique Dupin conic C'_i , i.e., a homothetic copy of C , that circumscribes each triangle \bar{t}_i (Figure 8, left). The center of C'_i is called the *Dupin center* of t_i . Clearly, the six conics C'_i are translational copies of each other, since the triangles \bar{t}_i are congruent and are translational or reflectional copies of each other (Figure 8, middle). Then the Dupin centers of the six triangles \bar{t}_i form a centrally symmetric hexagon \bar{f} on the tangent plane Γ . We will call \bar{f} the Dupin hexagon (Figure 8, right). This procedure of computing the Dupin centers of the triangles and connecting them into a hexagon will be referred to as *Dupin duality*.

We stress that Dupin duality is defined in the tangent plane of S and equipped with the Dupin indicatrix of S at the tangent point.

Since perturbation errors are incurred from mapping the vertices v_i of the original triangle mesh T of the surface S to \bar{v}_i , the Dupin duality is an approximation to the tangent duality. The following proposition ensures that it is indeed a good approximation. The proof of the proposition is given in the appendix.

Proposition 2 *Suppose that the size of the triangles t_i of T is $O(h)$. Then there is an $O(h^2)$ difference between each vertex u_i of the hexagon face f of H generated by the tangent duality and its corresponding vertex \bar{u}_i of the Dupin hexagon \bar{f} generated by the Dupin duality.*

The simplicity of the Dupin duality makes it easy to analyze the properties of the tangent duality. We will see how it can be used to derive simple conditions for avoiding self-intersections of the faces of P-Hex meshes. Since, by Proposition 2, the Dupin duality models faithfully the behavior of the tangent duality, these conditions are applicable asymptotically when computing P-Hex meshes using the tangent duality or its variants, provided that the triangles of T are sufficiently small in size.

The next proposition states a useful property of the Dupin hexagon. Its proof is elementary so is omitted.

Proposition 3 *The Dupin hexagon \bar{f} is inscribed in a Dupin conic. Furthermore, this Dupin conic is congruent to the Dupin conics of the six triangles \bar{t}_i in the triangle star \bar{T} . (See Figure 8, right.)*

4.2 Shape control

Avoiding P-Hex faces with self-intersection A P-Hex mesh is of little use if its faces have self-intersection. A face of a P-Hex mesh is *valid* if it has no self-intersection, i.e., it is a simple hexagon. A P-Hex mesh is *valid* if all its faces are valid. Accordingly, a triangle mesh approximating a surface S is said to be *valid* if it corresponds to a valid P-Hex mesh via the tangent duality. Similarly, in Dupin duality, a triangle star \bar{T} is said to be *valid* if the corresponding Dupin hexagon \bar{f} has no self-intersection. In the following we are going to derive conditions on a valid triangle star \bar{T} .

Proposition 4 *Suppose that the Gaussian curvature $K > 0$ at $v_c \in S$. Then the following are equivalent: 1) the triangle star \bar{T} is valid; 2) the Dupin center of the fundamental triangle \bar{t} is inside \bar{t} ; 3) the three edge directions of \bar{t} are not enclosed by any pair of conjugate directions with respect to the Dupin indicatrix C .*

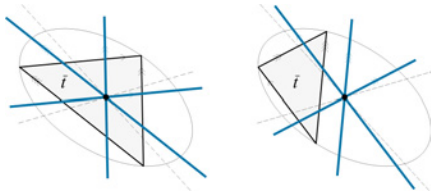


Figure 9: Illustration of the conditions in Proposition 4 for the case of $K > 0$. The dashed lines are a pair of conjugate directions. The three blue lines, parallel to the sides of \bar{t} , stand for the edge directions of \bar{t} . (Left) the edges directions are not enclosed by any conjugate directions; (right): the edges directions are enclosed by the two conjugate directions shown.

The proof of Proposition 4 is given in the Appendix. Figure 9 illustrates the conditions in Proposition 4. For a hyperbolic region, recall that there are two asymptotic directions at a hyperbolic point

of a surface [Struik 1988]. These two directions are self-conjugate. The next proposition gives a condition on a valid triangle star \bar{T} at a hyperbolic point of a surface. Its proof is given in the Appendix.

Proposition 5 *When the Gaussian curvature $K < 0$, the following are equivalent: 1) the triangle star \bar{T} is valid; 2) the three vertices of fundamental triangle \bar{t} are on different branches of its circumscribing Dupin hyperbola; 3) the three edge directions of \bar{t} are not all enclosed in the same range bounded by the two asymptotic directions of S at v_c .*

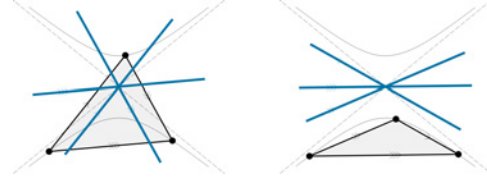


Figure 10: Illustration of the conditions in Proposition 5 for the case of $K < 0$. The three blue lines are parallel to the edge directions of the fundamental triangle. (Left) the edges directions are not enclosed by the asymptotical directions (dashed lines); (right): the edges directions are enclosed by the asymptotical directions.

Figure 10 illustrates the conditions in Proposition 5. Figure 11(top) shows a triangle mesh that does not meet the conditions in Proposition 5, with its invalid corresponding P-Hex mesh (i.e., having faces with self-intersection). Figure 11(bottom) shows a triangle mesh that satisfies the conditions in Proposition 5, with its valid corresponding P-Hex mesh.

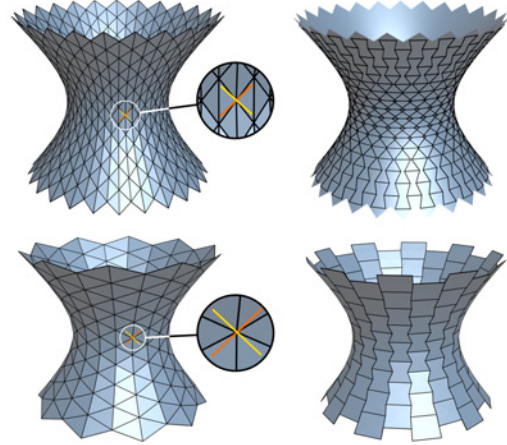


Figure 11: (Top): The condition (3) of Proposition 5 is not satisfied by the triangle mesh on the left, and the resulting P-Hex mesh on the right contains self-intersecting faces. (Bottom): the condition is satisfied by the triangle mesh and the resulting P-Hex mesh does not have face self-intersection.

Optimal shape of P-Hex faces From an aesthetic viewpoint, we would like to obtain those triangle meshes whose Dupin dual are valid P-Hex meshes with nicely shaped faces. When the Gaussian curvature $K > 0$, a natural criterion is to have, as much as possible, P-Hex faces to be images of a regular hexagon under affine transformations, or called affine regular hexagons, as shown in Figure 12(left). Evidently, this amounts to requiring that the Dupin center of the fundamental triangle \bar{t} be at the centroid of the fundamental triangle \bar{t} ; such a triangle is called an *ideal triangle* when $K > 0$.

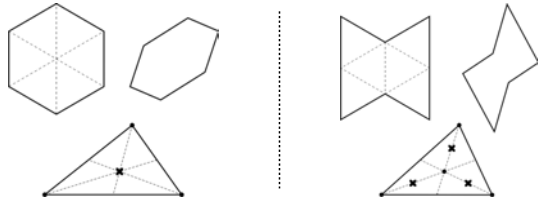


Figure 12: Left ($K > 0$): a regular hexagon and an affine regular hexagon. Right ($K < 0$): a quasi-regular hexagon and an affine quasi-regular hexagon.

When $K < 0$, we would like to have, as much as possible, the P-Hex faces to be affine copies of a *quasi-regular hexagon* which is formed by juxtaposing the two halves of a regular hexagon as shown in Figure 12(right). It is easy to show that this happens when the Dupin center of the fundamental triangle \bar{t} is at the midpoint of the centroid of t and any one of its three vertices, shown at the marked points in Figure 12(right). Such a triangle is called an *ideal triangle* when $K < 0$. That there are three possible locations for the Dupin center of an ideal triangle reflects the fact that the plane tiling with a quasi-regular hexagon is not invariant under rotation of $\pi/6$, in contrast to the case of plane tiling using a regular hexagon.

If the Dupin center is off the *ideal* locations defining ideal triangle, the shape of the resulting P-Hex face will deviate from an affine regular hexagon or an affine quasi-regular hexagon. However, according to Propositions 4 and 5, as long as the Dupin center stays inside the fundamental triangle \bar{t} , the resulting P-Hex face will be free of self-intersection.

5 Triangulation algorithms

For computing a P-Hex mesh of a given shape, our algorithm consists of three main steps: 1) compute a valid triangulation T of S ; 2) convert T into a nearly P-Hex mesh \bar{H} using Dupin duality; 3) apply optimization to turn \bar{H} into a P-Hex mesh H . In this section we shall explain the first two steps in detail.

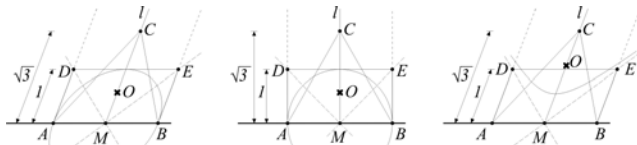


Figure 13: Construction of an ideal triangle $\triangle ABC$. (Left, $K > 0$): the Dupin indicatrix is an ellipse; (middle, $K > 0$): the Dupin indicatrix is a circle; (right, $K < 0$): the Dupin indicatrix is a hyperbola.

5.1 Computing ideal triangles

We first explain how to compute an ideal triangle. Suppose $K > 0$ and consider an ideal triangle $t : \triangle ABC$, i.e., its Dupin center is at its centroid O (Figure 13, left). Since the line CO passes through the midpoint M of the line segment \overline{AB} , it is conjugate to AB at M . Based on this observation we can determine the vertex C when A and B are given. First note that, given the Dupin indicatrix, there is a unique Dupin ellipse e that has \overline{AB} as its diameter. Let ℓ be the line conjugate to AB and passing its midpoint M . Construct the parallelogram $ABED$ with $AD \parallel BE \parallel \ell$ such that DE is tangent to the ellipse e . We note that the directions MD and ME are conjugate. Now mark point C on the line ℓ such that the length $|CM| = \sqrt{3}|AD|$. Then $\triangle ABC$ has its Dupin center at its centroid,

i.e., it is an ideal triangle. This can be seen by noting that obviously this construction works correctly when e is a circle (Figure 13, middle) and that the properties involved in the construction are affinely invariant. Here, any point C' on the line ℓ above the line DE defines a valid triangle $\triangle ABC'$, since in this case its three edge directions are not enclosed by any pair of conjugate directions with respect to the Dupin ellipse e . (cf. Proposition 4).

When $K < 0$, we apply the same construction as above for the case of $K > 0$, but with the difference that the two vertices D and E of the parallelogram $ABED$ are now determined such that MD and ME are on the asymptotes of the Dupin hyperbola centered at M . See Figure 13(right). Here the choice of C using the same rule $\|CM\| = \sqrt{3}\|AE\|$ ensures that $\triangle ABC$ is an ideal triangle, i.e., its Dupin center is located at $O = (A + B + 4C)/6$. The proof for the correctness of this construction is elementary, so is omitted. Again, any point C' above the line DE defines a valid triangle $\triangle ABC'$, since its three edge directions are not enclosed by the two asymptotic directions (cf. Proposition 5).

5.2 Computing a valid triangulation

We shall present two methods for laying valid triangulations on a surface S based on conjugate curve networks.

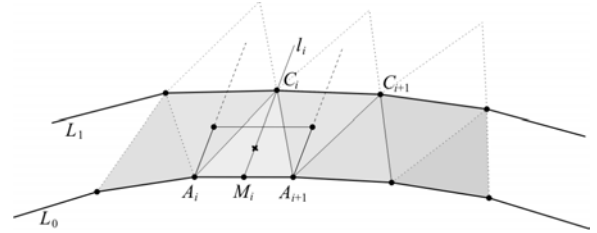


Figure 14: Laying triangles with the progressive conjugation method.

Method 1: Progressive conjugation method We start with a base curve L_0 with uniformly spaced sample points A_i on it, $i = 0, 1, 2, \dots, n$. (See Figure 14.) Let M_i denote the midpoint of the line segment $\overline{A_i A_{i+1}}$. Let ℓ_i be the half line starting at M_i and going in the direction conjugate to $\overline{A_i A_{i+1}}$. We use the procedure in Section 5.1 to find a point C_i on each ℓ_i such that $\triangle A_i A_{i+1} C_i$ is an ideal triangle (cf. Figure 13). Then connect all the segments $\overline{C_i C_{i+1}}$ to get the triangle $\triangle C_i C_{i+1} A_{i+1}$ to complete the first layer of triangles. Next, taking the poly-line $\mathcal{C} : \dots C_{i-1} C_i C_{i+1} \dots$ as the new base curve L_1 with the new sample points $A_i := C_i$, we follow the same procedure to fill the next layer of triangles. This is repeated to generate the subsequent layers.

The above family of curves L_i , $i = 0, 1, \dots, n$, is conjugate to the family of curves along the directions of ℓ_i (see Figure 14). Since this conjugate network is generated on-the-fly while the triangulation is being computed, the method is called *progressive conjugation method*. This method ensures that the resulting P-Hex faces are nearly affine regular or quasi-regular hexagons, since ideal triangles are computed within discretization errors (see Figure 15, left). A problem with this approach is that the widths and orientations of the triangle layers cannot easily be predicted or controlled. This leads to the following alternative that computes the triangulation following two pre-specified conjugate direction fields.

Method 2: Pre-specified conjugation method Here we consider laying a valid triangulation on a surface S parameterized by $P(u, v)$, $(u, v) = [u_0, \bar{u}] \times [v_0, \bar{v}]$ along two input conjugate direction

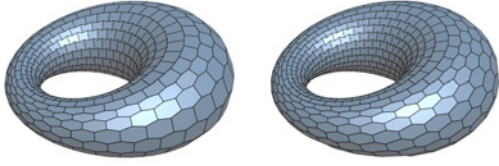


Figure 15: (Left): A triangulation and its P-Hex mesh computed using the progressive conjugation method (method 1), where the P-Hex faces are nearly affine regular (or quasi-regular) hexagons; (right) the results obtained using the pre-specified conjugation method (method 2).

fields $D_F : F(u, v)$ and $D_G : G(u, v)$. The first field D_F may be specified by the user and then the second field D_G is uniquely determined by D_F , assuming that the Gaussian $K \neq 0$. We first take the base curve L_0 to be a flow line from the first field D_F and sample points A_i on L_0 . (See Figure 16.) Let M_i be the middle point of the line segment $\overline{A_i A_{i+1}}$. There is a unique flow line ℓ_i from the second direction field D_G that passes through M_i . On each ℓ_i , following the procedure in Section 5.1 we find the point C_i such that $\triangle A_i A_{i+1} C_i$ is an ideal triangle. This is possible because D_F and D_G are conjugate, so the direction of ℓ_i is conjugate to that of $\overline{A_i A_{i+1}}$. Since the poly-line $\mathcal{C} : \dots C_{i-1} C_i C_{i+1} \dots$ is in general not a flow line from the field D_F , we select a flow-line L_1 from D_F to approximate the poly-line \mathcal{C} and use the intersections C'_i of the lines ℓ_i and the flow line L_1 as the final choices to define the triangles $\triangle A_i A_{i+1} C'_i$ and $\triangle C'_i C'_{i+1} A_{i+1}$, to complete the first layer of triangles. Note that L_1 should be computed such that its intersections C'_i with the lines ℓ_i are above the edge DE as shown in Figure 13; otherwise self-intersecting P-Hex faces would occur. By using L_1 as the new base curve with the new sample points $A_i := C'_i$, we proceed to complete the subsequent layers of triangles. With this pre-specified conjugation method we can ensure that the triangles are arranged along pre-specified conjugate directions, but due to this constraint the faces of the resulting P-Hex mesh may deviate from affine regular or affine quasi-regular hexagons.

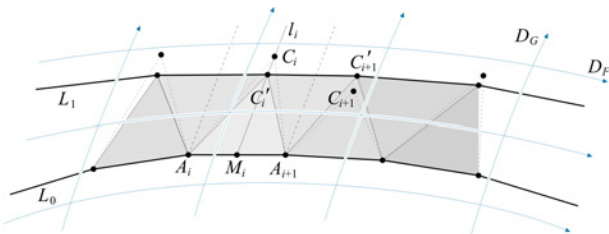


Figure 16: Laying triangles with the pre-specified conjugation method.

5.3 Degenerate cases ($K = 0$)

Free-form surfaces often contain parabolic points, i.e., points with $K = 0$, which is the case we have not considered so far in triangulation computation. If $K \equiv 0$ on S , then S is a plane or a developable surface [Carmo 1976]. The case of S being a plane is trivial, since any hexagonal mesh of S is a P-Hex mesh. When S is a developable, we just need to tile quadrilateral-shaped hexagons along the rulings of S (cf. the last paragraph of Section 3).

In the following we shall explain how to compute a valid triangulation across parabolic curves on a surface. Suppose that we reach a point at or near a parabolic curve on S when we compute a triangulation of S using either of the two methods in Section 5.2. In

general, the scheme in Section 5.1 for computing an ideal triangle will fail, because the step size MC will be either too large or too small. For example, if we lay the triangulation from bottom up for the surface in Figure 17(left), the step size will be too large near the parabolic curve, where the zero principal curvature direction points across the parabolic curve. In such a case, we re-use the valid step size from the previous layer where $K \neq 0$ so we can safely cross the parabolic curve. Figure 18(left) shows the triangulation of the vase generated using this scheme, together with the resulting P-Hex mesh.

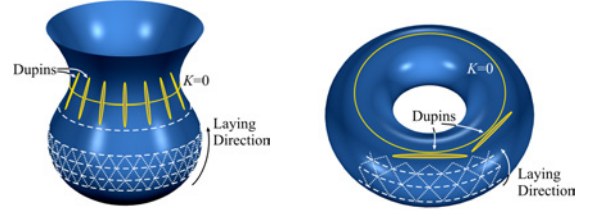


Figure 17: Two typical cases of parabolic curves, where $K = 0$.

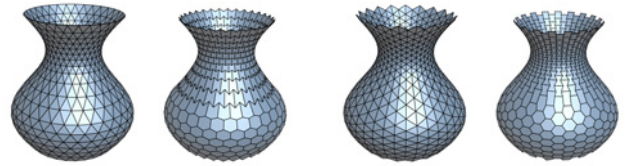
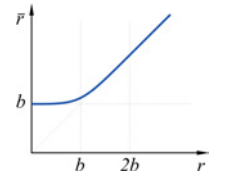


Figure 18: (Left): Triangulation and its P-Hex mesh of a vase using the step control scheme from bottom up; (right): a triangulation and its P-Hex mesh of the vase computed in the longitudinal direction.

At a point near or on a parabolic curve, the step size may also be too small or even zero. For example, this occurs if we lay out a triangulation on the torus shown in Figure 17(right), following the indicated laying direction. Here the zero principal curvature is in a direction along the parabolic curve. Although a small step size is sufficient to yield a valid triangle, the resulting triangle layers would be too narrow and the corresponding P-Hex faces would have a large disparity in size with those neighboring P-Hex faces away from the parabolic curve.

We circumvent the problem by using an appropriate lower bound b on the aspect ratio $|CM|/|AB|$ of the triangle $\triangle ABC$, as shown in Figure 13, which reflects the step size in triangulation layout. Suppose that the computed step size $|CM|$ produces the ratio r . Then the actual ratio \bar{r} we use will be r if $r \geq 2b$, but $b + r^2/(4b)$ if $2b > r \geq 0$. This scheme ensures a lower bound on the step size $|CM|$ and provides a smooth transition of the step size when it approaches the lower bound, as shown on the right. Figure 19(right) shows the triangulation of a torus generated using this scheme, together with the resulting P-Hex mesh.



6 Optimization

Initialization via Dupin duality For a valid triangulation T on surface S that contains no zero-curvature point, the tangent duality provides a fast and precise method for turning T into a P-Hex mesh, without the need for nonlinear optimization. However, as we noted

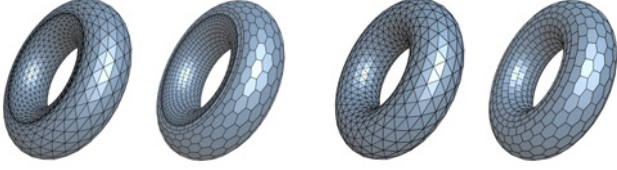


Figure 19: (Left): A triangulation and its P-Hex mesh of a torus computed without using a lower bound on the step size, leading to narrow triangle layers; (right): a triangulation and its P-Hex mesh of the torus computed using a lower bound on the step size.

earlier, the tangent duality construction may fail or become numerically unstable near a parabolic region or when the three vertices of triangle are too small. Hence, as a general treatment for free form shapes, we use an approximate Dupin duality to first convert T into a *nearly planar* hexagonal mesh \tilde{H}_0 , which, as a good initial mesh, is then made into a P-Hex mesh by our planarity optimization method.

We adopt the following notation. For a triangle face $\Delta v_1 v_2 v_3$, let $\kappa_{i,1}, \kappa_{i,2}, \vec{U}_i, \vec{V}_i$, and K_i denote the principle curvatures and their directions, and the Gaussian curvature at v_i . Let N_i denote the unit normal vector at v_i . The algorithm for computing the Dupin center for each triangle face is as follows.

- (1) *Parabolic region detection:* if K_1, K_2, K_3 are not of the same signs or one of $|K_1|, |K_2|, |K_3|$ is near zero (10^{-8}), then triangle $\Delta p_1 p_2 p_3$ in a parabolic region. We set the Dupin center of $\Delta v_1 v_2 v_3$ at its centroid, $(v_1 + v_2 + v_3)/3$.
- (2) For each vertex v_i in $\Delta v_1 v_2 v_3$, we project the other two vertices v_j, v_k onto the plane Γ_i determined by v_i and N_i . We use the curvature information to compute a Dupin conic C_i on Γ_i to pass through p_i and the projections of v_j, v_k . The center u_i of C_i is assigned to be the Dupin center associated with v_i .
- (3) The average center $u = (u_1 + u_2 + u_3)/3$ is assigned as the Dupin center of $\Delta v_1 v_2 v_3$.
- (4) Finally, a hexagonal mesh \tilde{H}_0 , with vertices $\{u_i\}_{i=0}^n$ and faces $\{f_i\}_{i=0}^m$, is obtained from the Dupin centers of all the triangles using a simple mesh-duality technique.

Planarity Optimization The computation of the hexagonal mesh \tilde{H}_0 is a close approximation to the Dupin duality on a tangent plane (cf. Section 4.1). Therefore, by Proposition 2, \tilde{H}_0 is nearly planar. From the numerical optimization point of view, \tilde{H}_0 is a good initial mesh for planarity optimization. The planarity of a face $f_i = u_0 u_1 u_2 u_3 u_4 u_5$ can be attained by forcing the volume of the tetrahedra formed by all the 4-point subsets of the vertices of f_i to be zero. Let $\text{vol}(u_i, u_j, u_k, u_\ell)$ denote the volume of a tetrahedron (u_i, u_j, u_k, u_ℓ) . Hence, for each hex-face f_i , we define the planarity constraint as

$$F(f_i) := \sum_{i=0}^5 \text{vol}^2(u_i, u_{i+1}, u_{i+2}, u_{i+3}) = 0.$$

with the indices modulo 6. To ensure minimal shape distortion, we add two energy terms into our optimization function: $F_s = \sum_{i=0}^n \|u_i - u_{i,0}\|^2$ and $F_d = \sum_{i=0}^n \text{dist}^2(u_i, \mathbf{S})$ Where $u_{i,0}$ is the initial position of the vertex u_i and \mathbf{S} is the underlying surface approximated by a triangular mesh. We use a penalty method to solve this constrained optimization problem [Nocedal and Wright 2006]. Therefore, the objective function is

$$\sum_{i=0}^m F(f_i) + \lambda F_s + \mu F_d.$$

We use the Gauss-Newton method to minimize this function. For most of our examples, we choose $\lambda = 1.0, \mu = 0.0$ and $\lambda_{(j+1)\text{-th step}} = 0.1 \lambda_{j\text{-th step}}$. Since the initial hexagonal mesh M_0 is almost planar, our optimization runs very fast. Normally, we have $\max_i \|F_p(f_i)\| = 10^{-15}$ within 10 iterations. The total time, including processing the conjugate curve network and optimization for planarity is from seconds to several dozens of second for most of the examples in this paper, depending on the number of faces. For example, the cyclide P-Hex mesh for the architectural model on the title page was computed in 10 seconds.

7 Experiments and discussions

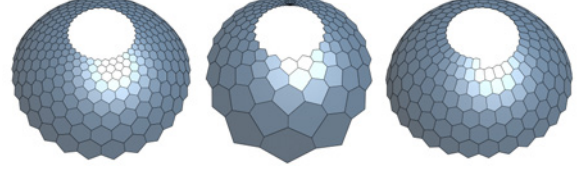


Figure 20: Three P-Hex meshes of different patterns on a spherical surface: radial, diverging, and spiral. Here, despite the variations in the face size, the P-Hex faces are controlled to be nearly affine regular hexagons.

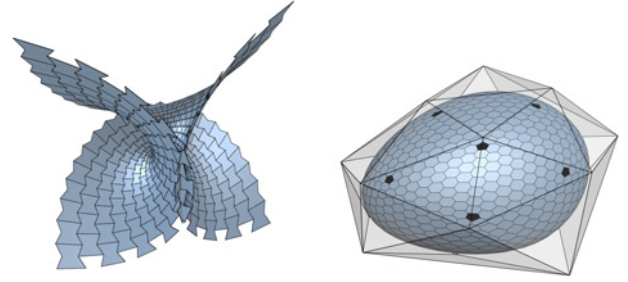


Figure 21: (Left): The P-Hex mesh of a minimal surface computed using the pre-specified conjugation method; (right) a convex P-Hex mesh whose triangulation under the Dupin duality is generated by applying Loop's subdivision to the shown control structure. The marked faces are pentagons.

In our algorithms the laying directions for computing a valid triangulation follow conjugate curve networks (see Section 5.2). Using different conjugate networks for computing a valid triangulation, P-Hex meshes of different patterns can be generated on the same surface Figure 20. Since, a P-Hex mesh has three distinct principal directions along which its faces can be aligned, it is important to arrange the conjugate network in coordination with those geometrically significant directions on S , in order to produce a good P-Hex mesh. For instance, in a negatively curved region, one should keep away from asymptotic directions, which are self-conjugate, highly distorted P-Hex faces would result.

In this regard, whenever possible, it is often desirable to adopt the curvature lines as the conjugate network for computing the triangulation, which offers the additional benefit of generating non-skewed affine regular (or quasi-regular) hexagonal faces, since the any two principal curvature directions are orthogonal. This is the choice made in generating the P-Hex meshes in Figure 15(right), Figure 18, and Figure 21. The two principal curvature directions are sometimes not equally good; for example, for the cyclide in Figure 15 or the torus in Figure 19, the show laying direction is the only feasible one. This is similar to the case of the P-Hex mesh of a

developable surface (cf. last paragraph of Section 3). For a freeform surface containing parabolic curves, the conjugate network should be designed to include the parabolic curve so that the triangulation is not “disrupted” when crossing the parabolic curve, as discussed in detail in Section 5.3. This is illustrated in Figure 22(right).

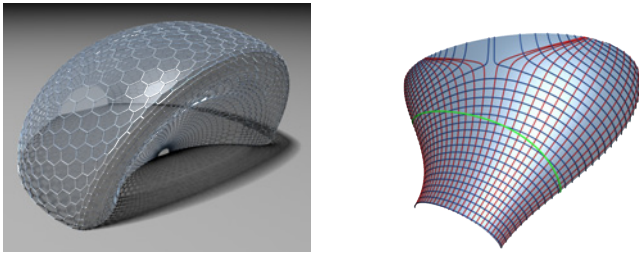


Figure 22: (Left): A free-form P-Hex mesh with smooth transition of the shape of P-Hex faces, computed using the pre-specified conjugation method; (right) curvature lines and the parabolic curve (in green) for the surface whose P-Hex mesh is shown at the bottom right of the figure at the top of page 1.

Not all surfaces can be tiled by P-Hex meshes. For example, it is well known that, as the consequence of Euler’s formula, a genus-0 surface cannot be represented by a hexagonal mesh with all valence-3 vertices. More specifically, suppose that a surface of genus g is represented by a mesh M that has only valence-3 vertices and has F_5 pentagons, F_6 hexagons and F_7 heptagons, and no other types of faces. Then there is $F_5 - F_7 = 12(1 - g)$. A realization of this relationship is a soccer ball or the celebrated fullerene C60 (i.e., $g = 0$) with 12 pentagonal faces and 20 hexagonal faces. Computing a P-Hex mesh for a general surface with genus $g \neq 1$ is beyond the capability of our algorithms presented in Section 5.2, since the methods assume that a singularity-free conjugate network is available. However, for the important class of convex surface of $g = 0$, subdivision surface schemes provide an effective means for generating valid triangulations for the purpose of generating P-Hex meshes (see Figure 21). This subdivision works because it generates a convex regular triangle mesh surface (with isolated non-valence-6 vertices) from a convex control polyhedron. It is not difficult to see that the triangles of such a mesh contain their Dupin centers with respect to the subdivision limit surface. Hence, by Proposition 4, the corresponding P-Hex mesh is valid. Further study is needed for controlling the shape of the P-Hex faces via this subdivision approach and, of course, for extending it to the case of non-convex surfaces.

8 Conclusion and future work

We have studied the relationship between regular triangulations and P-Hex meshes. We focused on understanding the effects of surface curvature on the P-Hex faces, and provided characterization on those valid triangulations that lead to P-Hex meshes whose faces are free of self-intersection and have desired shapes, such as affine regular or quasi-regular hexagon. Based on this we developed a complete algorithm for computing valid triangle meshes and turning them into P-Hex meshes. For extensions to this work, our initial investigation (Figure 21(right)) points to the direction of introducing non-hexagon faces, in a controlled manner in terms of both location and number, to generate P-Hex-dominant meshes for surfaces with complex topology (i.e., high genus) or complex geometry.

References

ALLIEZ, P., COHEN-STEINER, D., DEVILLERS, O., LEVY, B., AND DESBRUN, M. 2003. Anisotropic polygonal remeshing. 485–493.

ALMEGAARD, H., BAGGER, A., GRAVESEN, J., JÜTTLER, B., AND ŠÍR, Z. 2007. Surfaces with piecewise linear support functions over spherical triangulations. In *Proceedings of Mathematics of Surfaces XII*, 42–63.

AURENHAMMER, F., AND KLEIN, R. 2000. Voronoi diagrams. In *Handbook of Computational Geometry*, J.-R. Sack and J. Urrutia, Eds. Elsevier, 201–290.

BOBENKO, A., AND SURIS, Y. 2005. *Discrete Differential Geometry: Consistency as Integrability*. arXiv math.DG/0504358.

BOBENKO, A. I., HOFFMANN, T., AND SPRINGBORN, B. A. 2006. Minimal surfaces from circle patterns: Geometry from combinatorics. *Annals of Mathematics* 164, 1, 231–264.

CARMO, M. D. 1976. *Differential Geometry of Curves and Surfaces*. Prentice Hall.

COHEN-STEINER, D., ALLIEZ, P., AND DESBRUN, M. 2004. Variational shape approximation. 905–914.

COXETER, H. S. M. 1989. *Introduction to Geometry*, second ed. New York, John Wiley & Sons, Inc.

CUTLER, B., AND WHITING, E., 2006. Constrained planar remeshing for architecture. Poster, Eurographics Symp. Geom. Processing.

GLYPH, J., SHELDEN, D., CECCATO, C., MUSSEL, J., AND SCHÖBER, H. 2004. A parametric strategy for freeform glass structures using quadrilateral planar facets. *Automation in Construction*, 187–202.

GRUNBAUM, B., AND SHEPHARD, G. C. 1986. *Tilings and Patterns*. W. H. Freeman and Company, New York.

HARRIS, P. J. F. 1999. *Carbon Nanotubes and Related Structures: New Materials for the Twenty-first Century*. Cambridge University Press.

KÄLBERER, F., NIESER, M., AND POLTHIER, K. 2007. Surface parameterization using branched coverings. *Computer Graphics Forum (Proceedings of Eurographics 2007)* 26, 3, 375–384.

KAWAHARADA, H., AND SUGIHARA, K. 2006. Dual subdivision - a new class of subdivision schemes using projective duality. In *The 14th International Conference in Central Europe on Computer Graphics, Visualization and Computer Vision*, 9–17.

LIU, Y., POTTMANN, H., WALLNER, J., YANG, Y., AND WANG, W. 2006. Geometric modeling with conical meshes and developable surfaces. *ACM Transactions on Graphics (Proceedings of SIGGRAPH 2006)* 25, 3, 681–689.

MARINOV, M., AND KOBBELT, L. 2004. Direct anisotropic quad-dominant remeshing. In *Proc. Pacific Graphics*, 207–216.

MUELLER, C. 2007. Mixed area of parallel polygons and discrete minimal surfaces. Tech. rep., Geometry preprint 07-04, TU Graz.

NOCEDAL, J., AND WRIGHT, S. J. 2006. *Numerical Optimization*. Springer.

OSWALD, P., AND SCHRÖDER, P. 2003. Composite primal-dual $\sqrt{3}$ -subdivision schemes. 135–164.

POTTMANN, H., ASPERL, A., HOFER, M., AND KILLIAN, A. 2007. *Architectural Geometry*. Bentley Institute Press.

POTTMANN, H., LIU, Y., WALLNER, J., BOBENKO, A., AND WANG, W. 2007. Geometry of multi-layer freeform structures for architecture. *ACM Transactions on Graphics (SIGGRAPH 2007)* 26, 3, Article No. 65.

SAUER, R. 1970. *Differenzgeometrie*. Springer-Verlag.

SEVERIANO, J. A. D., GONZALEZ, C. O., FERNANDEZ, R. T., AND DEL VAL, C. M. 2005. Power diagrams in the design of chordal space structures. In *The 2nd International Symposium on Voronoi Diagrams in Science and Engineering*. 93–104.

STRUİK, D. J. 1988. *Lectures on Classical Differential Geometry*, second ed. Dover Publications.

TARNAI, T. 1993. Geodesic domes and fullerenes. In *The Fullerenes*, H. W. Kroto and D. R. M. Walton, Eds. Cambridge University Press, 145–154.

TERRONES, H., AND MACKAY, A. L. 1992. The geometry of hypothetical curved graphite structures. In *The Fullerenes*. Pergamon Press.

THOMPSON, D. W. 1992. *On Growth and Form*. Cambridge University Press.

WEYL, H. 1983. *Symmetry*. Princeton University Press.

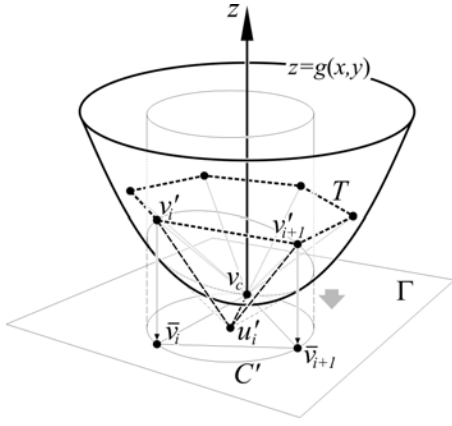


Figure 23: Local quadratic approximation of S .

Appendix

Proof of Proposition 2: Let T be a regular triangulation of the surface S with face size $O(h)$. We parameterize the surface S locally as a graph of a function $z = f(x, y)$ over the tangent plane Γ of S at a vertex $v_c \in S$ of T . In the 2D coordinate system on Γ with the x and y axes along the principal curvature directions and the origin at v_c , $z = f(x, y)$ is approximated by the quadratic function $z = g(x, y) \equiv \frac{1}{2}(\kappa_1 x^2 + \kappa_2 y^2)$ with an $O(h^3)$ error, where κ_1 and κ_2 are the principal curvatures of S at v_c , since $z = g(x, y)$ is the second order Taylor expansion of $z = f(x, y)$ (see Figure 23).

Due to the smoothness assumption on the regular triangulation and the second order approximation of the surface S by its Taylor approximation $z = g(x, y)$, it is easy to see that, with perturbations of $O(h^2)$, the vertices v_i , $i = 0, 1, \dots, 5$, of T that are adjacent to v_c can be moved to points v'_i on the surface $z = g(x, y)$ such that the vertical projections \bar{v}_i of the v'_i (i.e., along the z direction) onto the tangent plane Γ form a centrally symmetric hexagon $\bar{v}_0 \bar{v}_1 \bar{v}_2 \bar{v}_3 \bar{v}_4 \bar{v}_5$ with the triangles $v_c \bar{v}_i \bar{v}_{i+1}$ being congruent to each other, $i = 0, 1, \dots, 5$, modulo 6. Let $f' : u'_0 u'_1 u'_2 u'_3 u'_4 u'_5$ denote the hexagon on the plane Γ obtained by applying the tangent duality to the vertices v'_i on $z = g(x, y)$. Let $f : u_0 u_1 u_2 u_3 u_4 u_5$ denote the hexagon on Γ obtained by applying the tangent duality to the vertices v_i on $z = f(x, y)$, i.e., on the surface S . Since the errors between the v_i on S and the v'_i on $z = g(x, y)$ are $O(h^2)$, the different between their corresponding hexagons f and f' obtained via the tangent duality is $O(h^2)$.

Let $\bar{f} : \bar{u}_0 \bar{u}_1 \bar{u}_2 \bar{u}_3 \bar{u}_4 \bar{u}_5$ denote the hexagon on Γ obtained by applying Dupin duality to the vertices \bar{v}_i , $i = 0, 1, \dots, 5$ (Figure 7). To complete the proof, we are going to show that the hexagon \bar{f} is the same as the hexagon f' . Consider the triangle $\Delta v_c \bar{v}_i \bar{v}_{i+1}$ on $z = g(x, y)$, whose vertical projection on Γ is $\Delta v_c \bar{v}_i \bar{v}_{i+1}$ (see Figure 23). It is elementary to show the intersection point u'_i of the paraboloid $z = g(x, y)$ with the plane P_i containing $\Delta v_c \bar{v}_i \bar{v}_{i+1}$ is a conic whose vertical projection on Γ is the Dupin conic C'_i circumscribing $\Delta v_c \bar{v}_i \bar{v}_{i+1}$. Clearly, the intersection of the three tangent planes of $z = g(x, y)$ at v_c , v'_i and v'_{i+1} is the pole of the plane P_i with respect to $z = g(x, y)$ as a quadric surface. Since the vertical projection here is a stereographic projection on $z = g(x, y)$ with the center of projection at infinity in the direction of the z axis, the pole of P_i , i.e., u'_i , is identical with the center of the conic C'_i [Aurenhammer and Klein 2000], which is the Dupin center \bar{u}_i of $\Delta v_c \bar{v}_i \bar{v}_{i+1}$ (see Figure 7). This completes the proof. \square

Proof of Proposition 4: Given the triangulation \bar{T} and the Dupin indicatrix of S at v_c , the six vertices \bar{u}_i of the hexagon \bar{f} form two

triangles $\Delta r_1 r_2 r_3$ and $\Delta r'_1 r'_2 r'_3$, as shown in Figure 24(left). These two triangles are reflections and are both congruent with the fundamental triangle \bar{i} . Clearly, the hexagon \bar{f} is obtained by tracing the vertices r_i and r'_i in the order: $r_1 \Rightarrow r'_3 \Rightarrow r_2 \Rightarrow r'_1 \Rightarrow r_3 \Rightarrow r'_2 \Rightarrow r_1$.

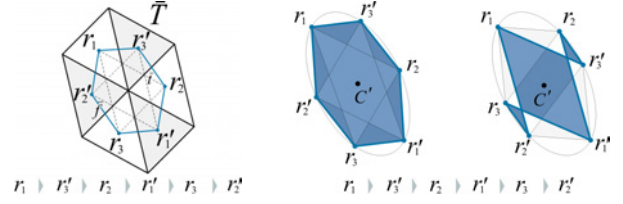


Figure 24: Illustration 1 for the Proof of Proposition 4.

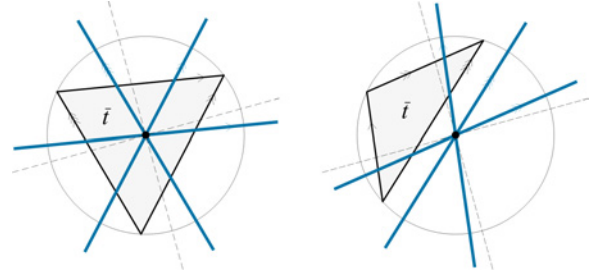


Figure 25: Illustration 2 for the Proof of Proposition 4. The dashed lines are a pair of conjugate directions. The three blue lines are translational copies of three edges at the Dupin center.

Let $\Delta r_1 r_2 r_3$ be identified with the fundamental triangle \bar{i} . By Proposition 3, the vertices r_i and r'_i lie on the same Dupin conic, denoted as C' , whose center is the Dupin center of $\Delta r_1 r_2 r_3$ (Figure 24, left). Since $K > 0$, C is an ellipse. First consider the special case of C' being a circle, for which two conjugate directions are orthogonal and the Dupin center of $\Delta r_1 r_2 r_3$ is its circumcenter. In this case, obviously the three edge directions of $\Delta r_1 r_2 r_3$ are not enclosed by any two orthogonal directions if and only if $\Delta r_1 r_2 r_3$ is an acute triangle, which holds if and only if the circumcenter of $\Delta r_1 r_2 r_3$ is inside $\Delta r_1 r_2 r_3$ (Figure 25, left). Since the properties used in this argument are preserved by affine transformation, we have shown that, in the general case of C being an ellipse, the three edges directions of $\Delta r_1 r_2 r_3$ are not enclosed by any two conjugate directions if and only if the Dupin center of the fundamental triangle $\bar{i} : \Delta r_1 r_2 r_3$ is inside $\bar{i} : \Delta r_1 r_2 r_3$.

Now we are back in the general case of C' being an ellipse. If the center of C' is inside $\bar{i} : \Delta r_1 r_2 r_3$, then the \bar{h} yielded by tracing the vertices $r_1 \Rightarrow r'_3 \Rightarrow r_2 \Rightarrow r'_1 \Rightarrow r_3 \Rightarrow r'_2 \Rightarrow r_1$ is convex hexagon, thus has no self-intersection (Figure 24:middle). If the center of C' is outside \bar{i} (see Figure 24, right), the same tracing order will yield a self-intersecting hexagon \bar{f} . Hence, \bar{T} is valid if and only if the Dupin center of the fundamental triangle \bar{i} lies inside \bar{i} . This completes the proof. \square

Proof of Proposition 5: Since $K < 0$, the Dupin conic C' of \bar{i} is a hyperbola. Similar to the discussion in the proof of Proposition 4 for the case of $K > 0$, the vertices of \bar{f} consists of the vertices of two triangles $\Delta r_1 r_2 r_3$ and $\Delta r'_1 r'_2 r'_3$, which are reflections of each other and are both congruent to the fundamental triangle \bar{i} of \bar{T} . Furthermore, \bar{f} is formed by tracing the vertices of $\Delta r_1 r_2 r_3$ and $\Delta r'_1 r'_2 r'_3$ in the same order: $r_1 \Rightarrow r'_3 \Rightarrow r_2 \Rightarrow r'_1 \Rightarrow r_3 \Rightarrow r'_2 \Rightarrow r_1$. Let us identify $\Delta r_1 r_2 r_3$ with \bar{i} . Obviously, the three edge directions of $\bar{i} : \Delta r_1 r_2 r_3$ are enclosed in a range bounded by the two asymptotes of C' if and only if the three vertices of $\bar{i} : \Delta r_1 r_2 r_3$ are the same branch of the hyperbola C' .

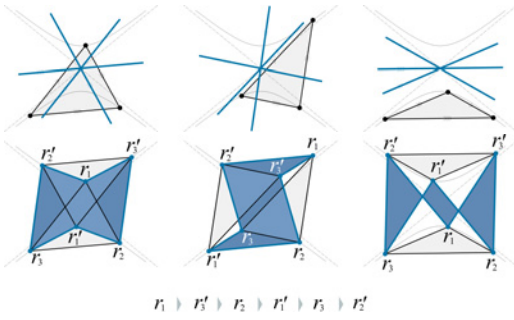


Figure 26: Illustration of the condition in Proposition 5. (Top): the dashed lines are the asymptotical directions. The three blue lines are parallel to the edge directions of the fundamental triangle. (Bottom): the corresponding Dupin hexagons.

First suppose that one of vertices of $\bar{t} : \triangle r_1 r_2 r_3$, say r_1 , is on one branch of C' , and r_2 and r_3 are on the other branch, as shown in Figure 26(left and middle). If r_1 is between r'_2 and r'_3 (Figure 26, left), by traversing the vertices $r_1 \Rightarrow r'_3 \Rightarrow r_2 \Rightarrow r'_1 \Rightarrow r_3 \Rightarrow r'_2 \Rightarrow r_1$, we obtain a simple, star-shaped, hexagon, shown as the shaded region in Figure 26(left). If r_1 does not lie between r'_2 and r'_3 on C' , following the required tracing order above still yields a simple non-convex hexagon, but it is no longer star-shaped (Figure 26:middle).

Next suppose that all the vertices of $\bar{t} : \triangle r_1 r_2 r_3$ lie the same branch of the hyperbola C' (Figure 26, right). Then, the vertices r'_i , as reflections of the r_i , are on the other branch of C' . Clearly, tracing these vertices in the required order $r_1 \Rightarrow r'_3 \Rightarrow r_2 \Rightarrow r'_1 \Rightarrow r_3 \Rightarrow r'_2 \Rightarrow r_1$ produces a self-intersecting hexagon, as shown in Figure 26(right). This completes the proof.